Comparative analysis of ChAdOx1 nCoV-19 and Ad26.COV2.S SARS-CoV-2 vector vaccines

Stephan Michalik
University Medicine Greifswald - Funktionelle Genomforschung
Florian Siegerist
University Medicine Greifswald
Raghavendra Palankar
Greifswald University Hospital
Kati Franzke
Friedrich-Loeffler-Institut
Maximilian Schindler
University Medicine Greifswald
Alexander Reder
University Medicine Greifswald
Ulrike Seifert
University Medicine Greifswald
Clemens Cammann
University Medicine Greifswald
Jan Wesche
Universitätsmedizin Greifswald, Transfusionsmedizin
Leif Steil
University Medicine Greifswald
Christian Hentschker
University Medicine Greifswald
Manuela Gesell-Salazar
University Medicine Greifswald
Emil Reisinger
Rostock University Medical Center
Martin Beer
Friedrich Loeffler Institute https://orcid.org/0000-0002-0598-5254
Nicole Endlich
University Medicine Greifswald
Andreas Greinacher
University Hospital Greifswald https://orcid.org/0000-0001-8343-7336
Uwe Völker (voelker@uni-greifswald.de)

University Medicine Greifswald https://orcid.org/0000-0002-5689-3448

Article

Keywords: SARS-CoV-2, vaccines, COVID-19, vector vaccines, medical research

DOI: https://doi.org/10.21203/rs.3.rs-736157/v1

Abstract

Vector-based SARS-CoV-2 vaccines have been associated with vaccine-induced thrombosis with thrombocytopenia syndrome (VITT/TTS), but the causative factors are still unresolved. We comprehensively analyzed ChAdOx1 nCov-19 (AstraZeneca) and Ad26.COV2.S (Johnson & Johnson). ChAdOx1 nCoV-19 contains significant amounts of host cell protein impurities, including functionally active proteasomes, and adenoviral proteins. In Ad26.COV2.S much less impurities were found. Platelet-factor 4 (PF4) formed complexes with ChAdOx1 nCoV-19 constituents, but not with purified virions from ChAdOx1 nCoV-19 or with Ad26.COV2.S. Vascular hyperpermeability was induced by ChAdOx nCoV-19 but not by Ad26.COV2.S.These differences in impurities together with EDTA-induced capillary leakage might contribute to the higher incidence rate of VITT associated with ChAdOx1 nCoV-19 compared to Ad26.COV2.S.

Introduction

Vaccination is key for the control of the SARS-CoV-2 pandemic. Adenoviral vector-, mRNA encapsulated in lipid nanoparticles-, and antigen-based vaccines are currently in use, all encoding the spike protein[1,2]. Since February 2021 the rare but severe adverse reaction of vaccine-induced immune thrombotic thrombocytopenia (VITT; synonym thrombosis with thrombocytopenia syndrome (TTS)) has been observed in individuals vaccinated against SARS-CoV-2. VITT/TTS occurs 5–20 days after vaccination with the ChAdOx1 nCoV-19 vaccine (AstraZeneca) and the Ad26.COV2.S vector vaccine (Janssen / Johnson & Johnson). The incidence rate of VITT/ TTS seems to be higher for ChAdOx1 nCoV-19. One case of VITT has been reported per 312,130 Ad26.COV2.S vaccinations in the United States (28 of 8,739,657 vaccinations, reporting through May 2021) compared to 1 per 73,665 ChAdOx1 nCoV-19 vaccinations (145 of 10,681,424 vaccinations, reporting through June 2021) in the United Kingdom. TTS/VITT involves high-affinity, platelet-activating anti-platelet factor 4 (PF4) antibodies[3–5], but the mechanisms triggering these anti-PF4 antibodies are still unresolved. VITT/TTS shows striking similarities with another PF4-mediated adverse drug effect, heparin-induced thrombocytopenia (HIT) and autoimmune HIT. In HIT, polyanions form complexes with PF4, inducing a conformational change, which triggers anti-PF4 antibodies. This immune response is pronounced in patients with tissue trauma and inflammation. We have shown that one or more constituents of the ChAdOx1 nCoV-19 vaccine interact with PF4. This might trigger conformational changes in the positively charged chemokine PF4 leading to the formation of a neoantigen and then subsequent activation of B-cells in a pro-inflammatory environment[6]. These activated B-cells produce high avidity anti-PF4 antibodies that bind PF4 and trigger an activation cascade of platelets and granulocytes, leading to NETosis and massive thrombin production. However, it is not known which vaccine components interact with PF4 and which additional factors influence this interaction.

Both vaccines (ChAdOx1 nCoV-19 and Ad26.COV2.S) are produced in human cell lines, T-REx-293 cells (human embryonic kidney cell, a HEK293 derivate) for ChAdOx1 nCoV-19 and PER.C6 TetR cells (human embryonic retinal cells) for Ad26.COV2.S, respectively. We and others have previously shown that the

vaccine ChAdOx1 nCoV-19 contains a large number of host cell proteins (HCP)[6,7]. Here we report the results of a comprehensive, comparative analysis of the ChAdOx1 nCoV-19 and Ad26.COV2.S vaccines, using proteomics, transmission electron microscopy, dynamic light-scattering, single-molecule light microscopy, and a capillary leakage assay.

Our data reveal substantial differences in composition and functional properties between both vaccines, which may contribute to the different incidences of TTS/VITT.

Results

Comparative profiling of ChAdOx1 nCoV-19 and Ad26.COV2.S vaccines

Comparative profiling of ChAdOx1 nCoV-19 and Ad26.COV2.S (three different LOTs each) consistently revealed significant differences: i) the total protein concentration of the ChAdOx1 nCoV-19 vaccine was approximately 3.4-times higher than the Ad26.COV2.S vaccine (mean: 102 ng/µl vs. 29.8 ng/µl) (Fig. 1a), ii) silver-nitrate staining of SDS-PAGE separated vaccines displayed a much more complex protein pattern for ChAdOx1 nCoV-19 than for Ad26.COV2.S (Fig. 1b). iii) mass spectrometric analysis (Suppl. Table 1) identified a much higher proportion (44.5 % to 59.2 % vs. only 0.26 % to 0.96 %; Fig. 1d, Suppl. Figure 1, 2) and number ($N_{ChAdOx1\ nCoV-19}$ = 1571 ± 31 vs. $N_{Ad26.COV2.S}$ = 59 ± 14; two-sided t-test p-value = 8.709e-06; Suppl. Figure 2) of host cell-derived human proteins (HCPs). A dilution series of a HEK293 cell line lysate confirmed the quantities of HCPs (54 % for ChAdOx1 nCoV-19 and 1.5 % for Ad26.COV2.S; Suppl. Figure 3). A laboratory HEK293 cell line was used instead of the cell line used for vaccine production. None of the top 10 most abundant human proteins in ChAdOx1 nCoV-19 was detected in Ad26.COV2.S (Suppl. Table 2). Adenoviral proteins comprised 40.8–55.5 % (ChAdOx1 nCoV-19) and 99.04–99.74 % (Ad26.COV2.S) of total ion intensity, while the SARS-CoV-2 spike protein was detected only in the ChAdOx1 nCoV-19 vaccine (n = 3 different LOTs; Suppl. Figure 1). Western blot analysis confirmed the significant abundance of eleven selected HCP-proteins in the ChAdOx1 nCoV-19 vaccine, which even exceeded the abundances detected in the HEK293 cell line. None of these proteins was detected in the Ad26.COV2.S vaccine.

In summary, per vaccine dose (500 µl) of ChAdOx1 nCoV-19 we estimated 19.13–33.81 µg HCP and 23.34–26.30 µg chimpanzee adenovirus proteins and for the Ad26.COV2.S vaccine 0.04–0.19 µg HCP and 10.25–19.23 µg adenoviral proteins. Since the ca. 5x10e10 virions per vaccine dose weigh about 12.5 µg, both vaccines contain unassembled virus proteins, mostly hexon proteins.

Proteasome activity in the different vaccines

Proteasome subunits were identified by mass spectrometry and verified by Western blot analysis (Fig. 2a, Suppl. File 1). Chymotrypsin-like activity associated with the proteasomal beta-5 subunit showed LOT-dependent high levels in ChAdOx1 nCoV-19, while in Ad26.COV2.S only minimal proteasome activity was found in one of three LOTs (Fig. 2b). Inhibition of the proteasome activity by 100 nM bortezomib[8] confirmed assay specificity (Fig. 2c).

PF4-vaccine cluster formation

PF4 is the key protein involved in the immune response causing VITT. We assessed the interaction of PF4 with the native vaccines and the purified adenoviral particles of ChAdOx1 nCoV-19, which were obtained by sucrose cushion and gradient ultracentrifugation. The purity of isolated ChAdOx1 nCoV-19 virions was confirmed by transmission electron microscopy (TEM) and silver-staining of 1D SDS-PAGE (Suppl. Figures 5 and 6).

DLS confirmed PF4-induced clustering of the non-purified ChAdOx1 nCoV-19 vaccine (Fig. 3a, left panel). The hydrodynamic diameter increased from 88 ± 2.4 nm up to 151 ± 12 nm and 320 ± 45 nm with 10 µg/mL and 50 µg/mL PF4, respectively (Fig. 3a, dose-dependency is shown in Suppl. Figure 7. This complex formation was reversible upon addition of unfractionated heparin. In contrast, the addition of PF4 (50 µg/mL) only marginally increased the particle size when incubated with purified virions from ChAdOx1 nCoV-19 (from 79.6 ± 10.3 nm to 86.7 ± 6.22 nm; p = 0.2404) (Fig. 3a, middle panel) or the Ad26.COV2.S vaccine (from 85.7 ± 2.2 nm to 91.3 ± 2.83 nm; p = 0.0620).

Complex formation of PF4 with the ChAdOx1 nCoV-19 vaccine was charge-dependent, as ChAdOx1 nCoV-19's negative charge (zeta potential − 27.5 ± 4.7) was neutralized by PF4. In comparison, both, purified ChAdOx1 nCoV-19 virions (zeta potential − 1.7 ± 4.7) and the untreated Ad26.COV2.S vaccine (zeta potential − 4.5 ± 5.7) showed only a minimal negative charge (Fig. 3b).

Consistent with DLS and as described before[6], PF4 induced the formation of electron-dense aggregates with ChAdOx1 nCoV-19 (Fig. 3c), which contained unassembled hexon protein (Suppl. Figure 8). In contrast, no comparable aggregates were detected after incubation of PF4 with purified virions from ChAdOx nCoV-19 (Fig. 3d) or the Ad26.COV2.S vaccine (Fig. 3e).

PF4 single-molecule density analysis using single-molecule localization microscopy (SMLM; Suppl. Figure 9, 10) revealed that PF4 clusters formed on or in close vicinity of ChAdOx1 nCoV-19 adenoviral hexon proteins (PF4 single-molecule density ratio 7.09 ± 1.38, Fig. 3f and i, arrowheads in Suppl. Figure 9), but not on Ad26.COV2.S (1.13 ± 0.14, p < 0.0001) or purified ChAdOx1 nCoV-19 virions (2.33 ± 0.44, p = 0.0115, mean ± SEM, Fig. 3g-i); p-values refer to comparison with ChAdOx1 nCoV-19.

ChAdOx1 nCoV-19 induced vascular hyperpermeability

To study the effect of the two vaccines and EDTA (100 µM present in ChAdOx1 nCoV19 vaccine) on vascular permeability, we used *in vivo* microscopy of transgenic zebrafish larvae expressing an eGFP-tagged plasma protein (gc-eGFP). Intramuscular injections (Suppl. Video 1) of 1 nL of 100 µM EDTA or ChAdOx1 nCoV-19 locally increased vascular permeability indicated by a significant leakage of eGFP from the intravascular to the intramuscular compartment that was not observed after injection of Ad26.COV2.S or physiological saline (Fig. 4).

Discussion

Our comprehensive analyses revealed major differences between ChAdOx1 nCoV-19 and Ad26.COV2.S vaccines. Confirming our previous observation, a high proportion of HCP (54%) was found in the ChAdOx1 nCoV-19 vaccine, but only a very low level of HCP in Ad26.COV2.S (1.5%). This observation suggests very different purification approaches for the two vaccines, with a more thorough purification of adenoviruses in Ad26.COV2.S. Such differences might be caused by the use of detergent treatment of the infected production cell culture, which will complicate subsequent purification strategies[9].

The two vaccines display differences in their ability to interact with PF4. While we confirmed the previously observed interaction of PF4 with ChAdOx1 nCoV-19, PF4 did not form distinct complexes with Ad26.COV2.S or purified ChAdOx1 nCoV-19 virion preparations, highlighting the role of impurities in ChAdOx1 nCoV-19 for the observed interactions[6]. Consistent with our findings in DLS, a recent study using cryo-electron microscopy of ChAdOx1 nCoV-19 established a possible electrostatic interaction of the positively charged PF4 and the negatively charged adenoviral hexon polypeptide[10] as a likely functional basis for the interactions. We now show that this interaction can be efficiently abrogated by purifying the intact adenoviral vector from the vaccine formulation. Thus, the pronounced PF4-affinity to ChAdOx1 nCoV-19 is likely enhanced by process-related impurities like HCPs or free adenoviral components mediating the interaction with PF4.

Addition of PF4 to purified ChAdOx1 nCoV-19 virions or to Ad26.COV2.S resulted in a slight increase in particle size, indicating charge-related binding of PF4 to the virions, as addition of heparin reduced the size again. Potentially, virions bound to platelets may trigger the conformational change in PF4. Several studies have shown the interaction of different adenovirus with platelets. We cannot exclude that also more complex interactions occur, when hexon proteins or the virions come into contact with lymphatic or plasma proteins and then form multimolecular complexes with PF4. In both scenarios, the very high numbers of adenovirus in both vaccines (approximately 5 x 10e10 per dose) may contribute to increasing the likelihood of such complex formations.

Antibody formation against PF4 is enhanced by antigen presentation in an inflammatory environment. Recently, we have shown that intramuscular injection of ChAdOx1 nCoV-19 leads to EDTA-induced capillary leakage, thus increasing the vaccine's intravascular distribution[6]. These observations were made using Mile's skin edema assay (intradermal injection). Our zebrafish model allows for intramuscular injections, which recapitulates the actual mode of vaccination. EDTA and ChAdOx1 nCoV-19 but not Ad26.COV2.S rapidly induced local vascular hyperpermeability. Such an increase of local capillary leakage might facilitate direct contact of the immune system with vaccine components, as does accidental intravascular administration of the vaccine as it has been proposed as a potential mechanism of a vaccine-induced misdirected immune response against platelet proteins by Nicolai *et al.*[11].

Interestingly, proteasome activity was detectable in both vaccines, albeit only low activity was found in only one LOT of Ad26.COV2.S compared to substantially higher proteasome activities in all LOTs of ChAdOx1 nCoV-19. This is of particular interest since Hauler et al., showed that adenoviral capsid proteins are intracellularly processed by proteasomal degradation which is mediated by the chaperone

p97/VCP[12]. In our proteomic analysis, we identified VCP as one of the top 5 most abundant proteins of the ChAdOx1 nCoV-19 vaccine (Suppl. Table. 1, Suppl. Table 2). Proteasomal degradation of adenoviral components such as the hexon polypeptide and/or HCPs might lead to a reduction in vaccine efficiency. Whether proteasomal activity may also create potentially immunogenic or immunoreactive neoantigens remains unresolved.

VITT/TTS clinically occurs after ChAdOx1 nCoV-19 and Ad26.COV2.S and is mediated by platelet-activating anti-PF4 antibodies. The current data indicate that adenovirus particles and free hexon proteins are the common features of both vaccines. We only observed complex formation of PF4 with ChAdOx1 nCoV-19. This indicates that an additional cofactor is needed, which is only present in the ChAdOx1 nCoV-19 vaccine, but may also allow formation of PF4 complexes, if present *in vivo* in the vaccinated individual.

Beyond VITT/TTS, the potential for alloantibody formation by protein contaminants in vaccines is a matter of concern since the PregSure® vaccine, used in cattle, induced bovine neonatal pancytopenia (BNP). BNP is a vaccine-induced alloimmune disease that was observed in young calves of PregSure® vaccinated cows and is characterized by hemorrhages, pancytopenia, and severe destruction of hematopoietic tissue. These alloantibodies had been likely induced by cell line contaminants of the vaccine as they cross-reacted with the bovine kidney cell line used for vaccine production[13]. VITT/TTS is an acute reaction occurring within two weeks after vaccination. Alloantibodies will only cause clinical effects in case of pregnancy or organ transplantation. Systematic screening of vaccinated individuals excluding or confirming such alloantibodies should be performed to clarify whether this theoretical concern requires further measures.

In summary, we show that process-related impurities in the form of HCP and active proteases are not a general feature of vector-based SARS-CoV-2-vaccines. More stringent purification strategies will reduce the complex formation of PF4 with vaccine constituents. EDTA-induced leakage and HCP impurities might explain the higher incidence rate of VITT/TTS for ChAdOx1 nCoV-19 compared to Ad26.COV2.S vaccines.

The authors would like to point out again that only the comprehensive vaccination of the human population can effectively contain the SARS-CoV-2 pandemic.

Materials And Methods

Sample preparation for LC-MS/MS analysis.

Vaccines were precipitated using a quantitative salt-acetone precipitation[14] and the precipitate was resuspended in one fifth of the initial volume using 20 mM HEPES buffer pH 8 containing 1 % (w/v) SDS.

Determination of protein concentrations was performed using a microBCA assay according to the manufacturer’s instructions (Pierce Thermo Fisher, Bonn, Germany).

2 µg of protein was reduced (2.5 mM DTT ultrapure, Invitrogen/Thermo Fisher, Bonn, Germany) for 30 minutes at 37 °C and alkylated (10 mM iodoacetamide for 15 minutes at 37 °C, Sigma Aldrich, Munich, Germany). Subsequently, protein was digested with trypsin (enzyme to protein ratio of 1:25) on SP3 beads as described by Blankenburg *et al.*[15].

SDS gel and Western blot analysis.

For protein separation, 2 µl of the three precipitated ChAdOx1 nCoV-19 (LOT 1 – 1.14 µg, LOT 2 – 1.05 µg, LOT 3 – 0.86 µg) and Ad26.COV2.S vaccine samples (LOT 1 – 0.39 µg, LOT 2 – 0.3 µg, LOT 3 – 0.2 µg) corresponding to one fiftieth of one vaccine dose as well as dilutions of HEK293 total protein lysate (1.5, 1.0, 0.5 and 0.25 µg) were adjusted to 10 µl sample volume with water and 4x SDS-PAGE sample buffer (Licor D00317-01) with added mercaptoethanol [10 %]. Accordingly, 0.5 µl of size standard (PageRuler Prestained Protein Ladder, Invitrogen/Thermo Fisher) was adjusted to a final volume of 10 µl with water and 4x SDS-sample buffer. Samples and standard were denatured for 2 min at 95 °C, chilled to room temperature and loaded to a precast NuPAGE™ 4 to 12 %, Bis-Tris Midi Gel 1.0 mm x 26 well (WG1403BX10, Invitrogen/Thermo Fisher). Electrophoresis was performed at 150 V using a Power Pack 200 (BioRad, Hercules, CA, USA) and a Criterion Cell (BioRad). All reagents and buffers were used according to the manufacturer's instructions. For the pure visualization of protein bands, silver nitrate staining was performed, as previously described by Shevchenko *et al.*[16]. Gel images were digitized using a digital camera.

The Western blots were prepared using the Trans-Blot Turbo Transfer System from BioRad. Proteins were transferred onto midi-size LF PVDF membranes for 10 min at 2.5 A and 25 V. The proper transfer of proteins to the PVDF membrane was verified and documented using LICOR's Revert Total Protein Stain protocol (Doc # 988-19494). Control stains were scanned using the Odyssey® CLx Imaging System (LI-COR Biosciences) in the 700 nm channel at 84 µm resolution, medium intensity and auto adjust. All further steps were followed according to the Western blot protocol of LI-COR (Doc # 988-19647). The detection of the specific proteins was performed with primary and secondary antibodies indicated in Table 1 using the respective incubation conditions. Detection of the specific signals was performed using the Odyssey® CLx Imaging System in the 800 nm channel at 84 µm resolution, medium intensity and auto adjust.

Supplemental Table 1: Used antibodies

Target	Primary antibody	Dilution and incubation conditions	Secondary antibody	Dilution and incubation conditions
HSP90-alpha class A member 1 (Entrez Gene ID 3320)	HSP90 Rabbit Polyclonal antibody IgG (Proteintech No: 13171-1-AP	1:4000 / room temperature / overnight	Licor Goat anti-Rabbit IRDye 800CW No. 926-32211	1:10000 / room temperature / 1 h
HSP90AB1class B member 1 (Entrez Gene ID 3326)	HSP90AB1 Rabbit Polyclonal IgG (Proteintech No: 11405-1-AP)	1:4000 / room temperature / overnight	Licor Goat anti-Rabbit IRDye 800CW No. 926-32211	1:10000 / room temperature / 1 h
GRP94-beta (Entrez Gene ID7184)	GRP94 Rabbit Polyclonal IgG (Proteintech No: 14700-1-AP)	1:4000 / room temperature / overnight	Licor Goat anti-Rabbit IRDye 800CW No. 926-32211	1:10000 / room temperature / 1 h
14-3-3-Epsilon (Entrez Gene ID 7531)	14-3-3-Epsilon Rabbit Polyclonal IgG (Proteintech No: 11648-2-AP)	1:4000 / room temperature / overnight	Licor Goat anti-Rabbit IRDye 800CW No. 926-32211	1:10000 / room temperature / 1 h
Tubulin alpha-1B (Entrez Gene ID 10376)	Tubulin alpha-1B Rabbit Polyclonal IgG (Invitrogen No PA5-21979)	1:3000 / room temperature / overnight	Licor Goat anti-Rabbit IRDye 800CW No. 926-32211	1:10000 / room temperature / 1 h
Histone H4 (Entrez Gene ID 8367)	Histone H4 Rabbit Polyclonal IgGG (Proteintech No: 16047-1-AP)	1:500 / 4°C/ overnight	Licor Goat anti-Rabbit IRDye 800CW No. 926-32211	1:10000 / room temperature / 1 h
YWHAZ (Entrez Gene ID 7534)	YWHAZ Rabbit Polyclonal IgG (Proteintech No: 14881-1-AP)	1:4000 / room temperature / overnight	Licor Goat anti-Rabbit IRDye 800CW No. 926-32211	1:10000 / room temperature / 1 h
Vimentin (Entrez Gene ID 7431)	Vimentin Rabbit Polyclonal IgG (Invitrogen No: PA5-27231)	1:10000 / room temperature / overnight	Licor Goat anti-Rabbit IRDye 800CW No. 926-32211	1:10000 / room temperature / 1 h
PSMA4 (Entrez Gene ID 5685)	20S Proteasome alpha4 (H-4)_ Mouse Monoclonal IgG (Santa Cruz Biotech., INC. No: sc-271297)	1:1000 / room temperature / overnight	Licor Goat anti-Mouse IRDye 800CW No. 926-32210	1:10000 / room temperature / 1 h
PSMB5 (Entrez Gene ID 5693)	PSMB5 (D1H6B) Rabbit Monoclonal IgG (Cell Signaling Technology No:12919)	1:1000 / room temperature / overnight	Licor Goat anti-Rabbit IRDye 800CW No. 926-32211	1:10000 / room temperature / 1 h
PSMB6 (Entrez Gene ID 5694)	PSMB6 (E1K9O) Rabbit monoclonal IgG (Cell Signaling Technology No: 13267)	1:1000 / room temperature / overnight	Licor Goat anti-Rabbit IRDye 800CW No. 926-32211	1:10000 / room temperature / 1 h

LC-MS/MS and data analysis.

LC-MS/MS experiments were performed on an Orbitrap Exploris^{TM} 480 mass spectrometer (Thermo Scientific, Bremen, Germany) coupled to an Ultimate^{TM} 3000 RSLCnano HPLC (Dionex/ Thermo Scientific, Waltham, MA, USA).

Chromatographic separation of tryptic peptides was achieved by a 60 min linear gradient using a binary buffer system that consisted of: 0.1 % (v/v) acetic acid in HPLC-grade water; 100 % ACN in 0.1 % (v/v) acetic acid with increasing concentrations of acetonitrile (7-25 % (v/v) in 0.1 % (w/v) acetic acid) on a reverse phase column (Accucore 150-C18, 25 cm x 75 µm, 2.6 µm C18, 150 Å), at a flow rate of 300 nL/min at 40 °C. The MS scans were carried out in a m/z range of 350 to 1200 m/z.

For data acquisition in data independent mode (DIA) (ChAdOx1 nCoV-19 or Ad26.COV2.S vaccine LOT analysis), precursor scans were acquired at a resolution of 120,000 and fragments at a resolution of 30.000 in 66 windows with 13 m/z and a window overlap of 2 m/z. For detailed information see Suppl. Table 2. The mass spectrometry proteomics data have been deposited to the ProteomeXchange Consortium via the PRIDE[17] partner repository with the dataset identifier PXD027344.

Supplemental Table 2: Parameters for LC-MS/MS analyses

reversed phase liquid chromatography (RPLC)	
instrument	Ultimate 3000 RSLC (Thermo Scientific)
trap column	75 µm inner diameter, packed with 3 µm C18 particles (Acclaim PepMap100, Thermo Scientific)
analytical column	Accucore 150-C18, (Thermo Fisher Scientific) 25 cm x 75 µm, 2,6 µm C18 particles, 150 Å pore size
buffer system	binary buffer system consisting of 0.1 % acetic acid in HPLC-grade water (buffer A) and 100 % ACN in 0.1 % acetic acid (buffer B)
flow rate	300 nl/min
gradient	linear gradient of buffer B from 2 % up to 25 %
gradient duration	60 min
column oven temperature	40 °C
Mass spectrometry	
instrument	Orbitrap Exploris™ 480
electrospray	Nanospray FlexTM Ion Source
operation mode	data-independent
Full MS	
MS scan resolution	120000
AGC target	3e6
maximum ion injection time for the MS scan	60 ms
Scan range	350 to 1200 m/z
RF Lens	50 %
Spectra data type	profile
dd-MS2	
Resolution	30,000
MS/MS AGC target	3e6
maximum ion injection time for the MS/MS scans	auto
Spectra data type	profile

microscans	1
isolation window	66
Fixed first mass	200
dissociation mode	higher energy collisional dissociation (HCD)
Normalized collision energy	30 %

The data were analyzed with Spectronaut version 14.10.201222.47784 (Biognosis, Zurich, Switzerland) in directDIA mode using the human Uniprot database (version 01/2021) with added SARS CoV2 spike protein (YP_009724390.1) sequence and protein sequences of ChAdOx1 nCoV-19 vector[9] consisting of chimpanzee adenovirus Y25[10] (NC_017825) with exchanged regions (E4ORF4, E4ORF6, E4ORF6/7) from human adenovirus 5 (AC_000008) for the ChAdOx1 nCoV-19 analysis. For the Ad26.COV2.S analysis we used a database comprised of human Uniprot database (version 01/2021) with added SARS CoV2 spike protein (YP_009724390. 1) sequence and protein sequences of hAd26 (Uniprot taxon identifier ID 46928) with exchanged regions (E4ORF6/7) from human adenovirus 5 (AC_000008).

Identifications were based on a precursor Q-value cut-off of 0.001 and a $FDR_{protein}$ of 0.01. The complete Spectronaut parameters are listed in Suppl. Table 3.

Supplementary Table 3: Spectronaut parameters.

Parameter level	Parameter	Setting
Peptides	Toggle N-terminal M	TRUE
Peptides	Min Peptide Length	7
Peptides	Max Peptide Length	52
Peptides	Missed Cleavages	2
Peptides	Digest Type	Specific
Peptides	Enzymes / Cleavage Rules	Trypsin/P
Data Extraction	MS1 Mass Tolerance Strategy	Dynamic
Data Extraction	MS1 Mass Tolerance Strategy - Correction Factor	1
Data Extraction	MS2 Mass Tolerance Strategy	Dynamic
Data Extraction	MS2 Mass Tolerance Strategy - Correction Factor	1
XIC Extraction	XIC IM Extraction Window	Dynamic
XIC Extraction	XIC IM Extraction Window - Correction Factor	1
XIC Extraction	RT IM Extraction Window	Dynamic
XIC Extraction	RT IM Extraction Window - Correction Factor	1
Modifications	Max Variable Modifications	5
Modifications	Select Modifications - fixed Modifications	Carbamidomethyl (C)
Modifications	Select Modifications - variable Modifications	Oxidation (M)
Calibration	MS1 Mass Tolerance Strategy	System Default
Calibration	MS2 Mass Tolerance Strategy	System Default
Identification	Machine Learning	Per Run
Identification	Precursor PEP Cutoff	1
Identification	Protein Qvalue Cutoff	0.01
Identification	Exclude Single Hit Proteins	FALSE
Identification	PTM Localization	TRUE
Identification	PTM Localization - Probability Cutoff	0.75
Identification	P-value Estimator	Kernel Density Estimator

Identification	Precursor Qvalue Cutoff	0.001
Identification	Single Hit Definition	By Stripped Sequence
Quantification	Interference Correction	TRUE
Quantification	Best N Fragments per Peptide	TRUE
Quantification	Best N Fragments per Peptide - Min	6
Quantification	Best N Fragments per Peptide - Max	10
Quantification	Quantity MS-Level	MS2
Quantification	Quantity Type	Area
Quantification	Data Filtering	Qvalue
Quantification	Data Filtering - Imputing Strategy	No Imputing
Quantification	Cross Run Normalization	FALSE
Workflow	MS2 DeMultiplexing	Automatic
Workflow	Run Limit for directDIA Library	-1
Workflow	Profiling Strategy	iRT Profiling
Workflow	Profiling Strategy - Profiling Row Selection	Minimum Qvalue Row Selection
Workflow	Profiling Strategy - Profiling Row Selection - Qvalue Threshold	0.001
Workflow	Profiling Strategy - Profiling Target Selection	Profile only non-identified Precursor
Workflow	Profiling Strategy - Profiling Target Selection - Identification Criterion	Qvalue
Workflow	Profiling Strategy - Profiling Target Selection - Threshold	0.001
Workflow	Profiling Strategy - Carry-over exact Peak Boundaries	FALSE
Workflow	Profiling Strategy - Unify Peptide Peaks Strategy	Select corresponding Peak

The Spectronaut unique protein iBAQ intensities (filtered for at least 3 peptides per protein with ion Qvalues < 0.001) were cleared for preparation contaminants (trypsin, keratin, dermicidin) used for a comparison of samples[18].

Data analysis and generation of plots was carried out using R[19] (version 4.0.2) depending on the tidyverse (version 1.3.0)[20] and scales (version 1.1.1)[21].

Purification of adenovirus particles from ChAdOx1 nCov-19

The first step was a sucrose cushion ultracentrifugation. 1 to 6 ml vaccine were diluted in buffer (phosphate buffer) to 15 ml and loaded slowly over 2 ml 15 % sucrose solution (phosphate buffered; 17 ml tube, opaque, Beckman Coulter) forming a layer and centrifuged at 20.000 rpm , 12 °C for 2 hours with SW32Ti rotor in a Beckman Coulter Optima L-100XP. The supernatant was discarded and the resulting pellet was layered with buffer (1/10 of the starting volume of the vaccine) and incubated overnight at 4 °C.

The second step was a sucrose gradient ultracentrifugation. The resuspended pellet was loaded on a 5 to 50 % sucrose gradient (phosphate buffered; 17 ml tube, ultra clear, Beckman Coulter) that was prepared the day before for equilibration. For centrifugation, the same conditions were used as mentioned above. The resulting distinct and adenovirus-rich band was isolated.

The last step was an ultracentrifugation for pelleting of adenovirus particles. The isolated band was diluted in buffer to 4 ml volume and centrifuged (4 ml tube, opaque, Beckman Coulter) at 12.000 rpm, 12 °C for 2 hours with SW60Ti rotor. The supernatant was discarded and the resulting pellet was layered with buffer (1/10 of the starting volume of the vaccine) and incubated overnight at 4 °C. Finally, the quality of preparation was analyzed by transmission electron microscopy as described below.

Phosphate buffer: 50 mM Na_2HPO_4*$2H_2O$ pH 7.4, 150 mM NaCl

Proteasome activity assays

ChAdOx nCoV-19, Ad26.COV2.S and HEK293 cell lysates were tested for proteasomal activity. HEK293 cells were gently lysed by repeated freeze-thaw cycles in buffer containing 10 mM Tris (pH 7.0), 25 mM KCl, 10 mM NaCl, 1.1 mM $MgCl_2$, 1 mM DTT, 10 % glycerol and protease inhibitor cocktail Complete (Sigma-Aldrich). Chymotrypsin-like activity was assessed in 50 µl vaccine or HEK293T cell lysate (0.25 µg) using 0.2 mM fluorescently tagged substrate Suc-LLVY-AMC (Bachem, Bubendorf, Switzerland). To confirm proteasomal activity 100 nM Bortezomib (Selleckchem, Houston, Texas, United States), an inhibitor of chymotrypsin-like activity, was added. The free AMC fluorescence was quantified with a fluorometer using a 380/460 nm filterset (Fluorescence spectrometer Infinite M200 Pro, software i-control1.7; TECAN, Männerdorf, Switzerland). Increase of fluorescence was measured over 2 hours. Proteasome turnover was determined by calculating the rise of the linear slope in the beginning of the measurement (substrate turnover (Δ RFU/min)).

Dynamic Light Scattering and Zeta Potential Measurements

All dynamic light scattering (DLS) measurements were performed in a fixed scattering angle Zetasizer Nano-S system (Malvern Instruments Ltd., Malvern, UK). The hydrodynamic diameter (nm) was measured

at 25 °C, and light scattering was detected at 173° and three repeating measurements consisting of 12 runs of 10 seconds each. Experimental data were collected from at least three independent experimental replicates. For all DLS measurements, non-purified ChAdOx1 nCoV-19, purified ChAdOx1 nCoV-19 and Ad26.COV2.S vaccine was diluted at a ratio of 1:10 in sterile-filtered 0.9 % NaCl supplemented with 4 mg/mL D(+) sucrose (RNase/DNase free; Cat. No. 9097.1, Carl Roth GmbH, Germany). Assessment of changes in the hydrodynamic diameter of ChAdOx1 nCoV-19 vector in the presence of PF4 was performed by incubating 10 and 50 µg/mL of human PF4 (Chromatec, Greifswald, Germany) with ChAdOx1 nCoV-19 vaccine at RT for five minutes before DLS measurements. For some titration experiments, either 1:10 diluted ChAdOx1 nCoV-19 or Ad26.COV2.S vaccine was incubated with increasing concentrations of PF4 from 1, 5, 10,15, 20, 25, and 50 µg/mL. Similarly, PF4 at a fixed concentration of 10 µg/mL was incubated with ChAdOx1 nCoV-19 vaccine with decreasing dilutions of 1:1000, 1:750, 1:500, 1:250, 1:100, 1:50. 1:25 and 1:10. Dissociation of complexes formed between ChAdOx1 nCoV-19 vector and added components was achieved by 1 IU/ml unfractionated heparin (UFH, Ratiopharm GmbH, Ulm, Germany).

Surface zeta potential (ζ, mV) was performed in folded capillary zeta cells (DTS1070, Malvern Instruments Ltd., Malvern, UK). It consisted of three runs, each with 20 measurements at a voltage set to 10 V.

Data analysis was performed using Zetasizer software, Version 7.13 (Malvern Instruments Ltd., Malvern, UK). Statistical analysis and data plots were prepared with GraphPad Prism version 9.0.0 for Windows. Differences between groups were considered significant after assessment by ordinary one-way ANOVA with Sidak's multiple comparisons test, with Alpha set to 0.05.

Immunoelectron microscopy and transmission electron microscopy

For transmission electron microscopy (TEM) the vaccine or the purified adenovirus particles was incubated with biotinylated PF4 (10 ng/ml in phosphate buffer; PF4-biotin) for at least one hour at room temperature. After that, the sample was transferred to formvar coated TEM grids (400 mesh, Plano GmbH), washed with phosphate buffer and blocked with phosphate buffer containing 1 % BSA. On the one hand, samples were labeled with an anti-Adenovirus mAb (Abcam, ab7428, 1:500) for 1 hour at room temperature and an anti-mouse gold conjugate (BBI Solutions, GMHL10, 10 nm, 1:50) as secondary antibody. On the other hand, the same samples were labeled with a streptavidin-gold conjugate (Sigma, 10 nm, 1:10) for the staining of PF4-biotin for 45 min at room temperature.

All grids were stained with 1 % phosphotungstic acid at pH 7.4 and analyzed with a Tecnai-Spirit transmission electron microscope (FEI, Eindhoven) at an accelerating voltage of 80 kV. The same procedure was used for preparing the controls, vaccine and PF4-Biotin.

For analysis of preparation quality after the purification of ChAdOx1 nCoV-19 the samples were transferred to formvar coated TEM grids (400 mesh, Plano GmbH), stained with 1 % phosphotungstic

acid at pH 7.4 and analyzed with a Tecnai-Spirit transmission electron microscope (FEI, Eindhoven) at an accelerating voltage of 80 kV.

Super Resolution Single Molecule Light Microscopy

Immunofluorescence Staining

10 µg/ml human PF4 (Chromatek, Greifswald, Germany) was incubated with 1:10 diluted ChAdOx1 nCoV-19 (AstraZeneca, LOTs ABV5443, ABW0018, ABV5297) or Ad26.COV2.S (Johnson and Johnson, LOTs 21C11-01, 21C10-01, XD955) in 2 mg/ml sucrose in 0.9 % injection-grade NaCl. After 5 minutes incubation at room temperature, 10 µl were spread on beforehand washed (subsequent sonication in 99 % EtOH, 17 % HCl in 50 % MeOH, ultrapure water, 99 % EtOH) 22x22mm #1.5 high-precision coverslips (VWR, Germany). Slides were air-dried at room temperature and fixed with 2 % electron microscopy-grade paraformaldehyde (Thermo Fisher Scientific) in 4 % sucrose-containing PEM-buffer (80 mM PIPES, 5 mM EGTA, 2 mM $MgCl_2$) for 5 min at room temperature. Slides were blocked with 2 % fetal bovine serum, 2 % bovine serum albumin, 0.1 % cold fish gelatin and 2 % normal goat serum in 1x PBS pH 7.4 for 45 min at room temperature. For detection of PF4, a mouse monoclonal IgG2b (RTO clone, Thermo Fisher, MA5-17639) diluted to 2 µg/ml in 2 % bovine serum albumin in 1x PBS pH 7.4, was incubated for 30 min at room temperature under gentle agitation. Bound primary antibodies were detected after several washes in 1x PBS using AlexaFluor 488-conjugated secondary antibodies (A11001, Thermo Fisher Scientific) at 1:500 dilution for 30 min at room temperature. For detection of the hexon polypeptide, a custom Cy5-conjugated (Lightning-Link Cy5 conjugation kit according to manufacturer's description (Novus Biologicals, 781-0010)) IgG2a antibody (abcam, ab7428) was incubated at 1 µg/ml in 2 % bovine serum albumin for 1 hour at room temperature. Slides were collected in 1x PBS and stored at 4 °C in the dark upon mounting and imaging. Antibody specificity was checked beforehand using secondary immunofluorescence with minus primary antibody control.

Direct stochastical optical reconstruction microscopy (dSTORM)

Before imaging, coverslips were washed in ultrapure water and 100 nm multi-fluorescent Tetraspek Beads (Thermo Fisher) were added in a 1:800 dilution in ultrapure water for 5 min at room temperature. After one wash in electron microscopy-grade water, coverslips were inversely mounted on depression microscopy glass slides (VWR, Germany) in Everspark dSTORM buffer (Idylle Labs, Paris, France) containing deoxygenized 100 mM mercaptoethanolamin hydrochloride (MEA) in TRIS buffer pH 8[22]. Coverslips were sealed airtight with TwinSil two-component dental silicone. Care was taken that mounting time did not exceed 30 seconds to minimize oxygenization of the buffer. Slides were imaged after between 1 hour and 1 week incubation with the imaging buffer and were stored at 4 °C in the dark.

For dSTORM imaging, a Zeiss Elyra PS.1 super resolution system was used with a temperature-controlled chamber set to 30 °C. To equilibrate instruments and reduce drift, the system was switched on at least two hours before imaging. Samples were equilibrated for at least 20 minutes in the imaging chamber. The objective used was a Zeiss, Apochromat, 63x, 1.4 NA TIRF objective, and emitted fluorescence was

projected on an Andor iXon 897 EMCCD camera with a 512x512 pixel chip, resulting in an effective pixel size of 160 nm. Areas of interest with at least two fiducial markers per field of view were selected using the epifluorescence mode. Z-drift compensation was performed with the Definite Focus system set on continuous compensation. During continuous TIRF-HP-illumination, the laser power was gradually increased to bleach fluorophores until steady-state single-molecule photoswitching was observed. 256x256 pixels frames were acquired at a framerate of 55 Hz with a manual gain set to between 20 and 40. Subsequently, 14,000 frames image sequences of the same field of views of the Cy5 and AF488 fluorophores were recorded, saved as .czi files and imported to FIJI[23] using the BioFormats importer. After import, raw data was saved as .nji files using the NanoJ core toolbox[24]. Raw single channel dSTORM data was initially drift-corrected with the built-in function of the NanoJ core plugin. Chromatic aberration between both channels was estimated on intensity-averaged frames of the drift-corrected data (to clearly visualize fiducial markers) and corrected on drift-corrected source data using the Channel Registration function of NanoJ core. After drift correction and sub-pixel channel registration, image sequences were cropped to 10,000 frames of 200x200 pixels before performing emitter-localization analysis. Cropped, drift-corrected and channel-registered data was exported with NanoJ core as .nji files.

For both channels, blinking events were detected, and x-y localized with the Thunderstorm algorithm[25] using normalized Gaussian fitting with a 3 px fitting radius, weighted least squares fitting method, an initial Sigma of 1.6 px and multi-emitter fitting analysis disabled. The resulting localization table was exported as .csv files and uncertainty- as well as sigma-filtered. Data was then density-filtered with a minimum distance radius of 50 nm with a minimum of 5 neighbors in the radius. The resulting localization data was visualized either using the built-in averaged shifted histograms function with 10x magnification or as well as the scatter plot function with 50x magnification (with herein hexon-localizations density-filtered with a minimum of 50 neighbors in a distance radius of 50 nm). Single-channel data was visualized using the inverted NanoJ-orange LUT or merged and exported using basic FIJI functions.

Image analysis

To analyze PF4-molecule aggregation on adenoviral capsid clusters, PF4 particle density in- and outside boundaries of adenoviral complexes were quantified. To automate this, an ImageJ1-macro script was developed. In brief, dual-channel 50x magnified single-molecule scatterplots were imported to FIJI, adenoviral clusters gaussian-blurred and thresholding-based binarized. A ring-like reference region outside (500 nm outside the adenoviral particles, width of 500 nm) of each complex was defined which did not contain adenoviral localizations. Then, PF4 localizations in each region of interest (ROI, inside adenoviral particles and outside on glass as internal reference) were counted and normalized to the ROI area as particle density. To account for preparation-based differences in local molecule density, PF4 density ratios of the matching ROIs (inside/outside AV) were calculated and normalized to the median of every groups outside ROI density ratio. ImageJ macro scripts are available on http://www.github.com/siegerist.

Statistical analysis and data visualization was performed with Prism 9.1.2 (GraphPad Software, San Diego, California USA): Normality was checked using Kolmogorov-Smirnov testing. For >2 groups and non-parametric data, differences between groups were checked using Kruskal-Wallis-test with Dunn's multiple comparison test. P-values are indicated in the respective plots, where not indicated, p-values were >0.05.

Zebrafish vascular permeability assay

Zebrafish maintenance was performed as described previously[26]. All experiments were performed in accordance with German animal protection law overseen by the "Landesamt für Landwirtschaft, Lebensmittelsicherheit und Fischerei, Rostock" of the federal state of Mecklenburg - Western Pomerania. In order to track vascular leakage, Tg(-3.5fabp10a:gc-eGFP)[27] (ZFIN-ID: ZDB-FISH-150901-8595) and Tg(-3.5fabp10a:gc-eGFP); mitfa$^{w2/w2}$ were used[28]. Larvae at five days post fertilization were anesthetized with 0.02% tricaine (MS-222, Sigma-Aldrich) and placed laterally on a custom-made agarose dish. As demonstrated in Suppl. Video 1, approximately 1 nl intramuscular injections of 0.9 % NaCl, 100 µM EDTA, ChAdOx1 nCoV-19 (LOT: ABV5297) and Ad26.COV2.S (Lot: XD955 and 21C10-01) were performed with glass capillaries (Femtotips I, Eppendorf AG, Hamburg, Germany) attached to a Transjector 5246 (Eppendorf AG) into four adjacent myotomes caudal of the cloaca in each larva. Afterwards, larvae were embedded laterally in 0.6 % agarose (LE agarose, Biozym, Hessisch Oldendorf, Germany) with the injection side facing up and covered with E3 medium containing 0.02 % tricaine. Imaging was performed with a P2-SHR Plan Apo 1x objective attached to a SMZ18 fluorescence stereomicroscope equipped with a motorized Z-drive (Nikon GMBH, Düsseldorf, Germany) and an X-Cite Xylis LED (Excelitas, Göttingen, Germany). Z-Stacks with 10 frames for each larva were acquired with 470 nm slice-to-slice distance with a 135x magnification in the caudal region at 0 and 10 min post injection (p.i.). Z-Stacks were converted to maximum intensity projections (MIPs) and stacks of two MIPs for both timepoints were created. Fluorescence intensity measurements were performed with 4 custom ROIs for each injected myotome. The same ROIs were used to obtain the fluorescence intensity of the adjacent caudal vein in order to calculate a muscle to vessel ratio. The t=0 of each larva served as normalizer for the 10 min p.i. ratio and displays the leakage of eGFP into the musculature. Creation of MIPs, Stacks and measurements were performed with ImageJ (National Institutes of Health, Bethesda, MD, USA)). Statistical analysis was performed in Prism 9.1.2 (GraphPad Software, San Diego, California USA). After checking gaussian-distribution with Kolmogorov-Smirnov test, differences between groups were checked using Kruskal-Wallis-test with Dunn's multiple comparisons.

Declarations

Acknowledgements

We thank Katrin Schoknecht for support in the proteomics analyses, Mandy Jörn for graphical design of EM micrographs. The study has been funded by the Deutsche Forschungsgemeinschaft (DFG, German Research Foundation) grants: 374031971 - A06 and A11-TRR240, 398967434 - SFB/TR261, A11 -

SFB877, P6 - KFO306, B8 - SFB841, and INST 2026/13-1 FUGG, the Ministerium für Wirtschaft, Arbeit und Gesundheit Mecklenburg Vorpommern (project COVIDPROTECT), „Structure and Function of the Proteasome System in Platelets“ GR2232/8_1 and SE 885/2-1, Leibniz WissenschaftsCampus – ComBioCat – W10/2018, the Südmeyer fund for kidney and vascular research (“Südmeyer-Stiftung für Nieren- und Gefäßforschung”) and the Dr. Gerhard Büchtemann fund, Hamburg, Germany.

Author contribution

S.M., F.S., R.P., K.F., A.R., U.S, C.C., J.W., L.S., C.H., M.G-S., M.B., N.E., A.G., U.V. conceived the research. S.M., F.S., R.P., K.F., A.R., U.S, C.C., J.W., L.S., C.H., M.G-S., M.B., N.E., A.G., U.V. defined the methodology. S.M., F.S., R.P., K.F., A.R., M.S., U.S, C.C., J.W., L.S., C.H., M.G-S. conducted the analysis. S.M., F.S., R.P., K.F., A.R., U.S, C.C., J.W., L.S., C.H., M.G-S., M.B., N.E., A.G., U.V. interpreted the data. S.M., F.S., R.P., K.F., A.R., M.S. generated data visualization. S.M., F.S., R.P., K.F., M.B., N.E., A.G., U.V. wrote the first draft of the manuscript. All authors contributed to the interpretation of results and manuscript editing. All authors approved the final version of the manuscript.

Competing interests statement

Dr. Greinacher reports personal fees and non-financial support from Aspen, grants from Ergomed, grants and non-financial support from Boehringer Ingelheim, personal fees from Bayer Vital, grants from Rovi, grants from Sagent, personal fees from Chromatec, personal fees and non- financial support from Instrumentation Laboratory, grants and personal fees from Macopharma, grants from Portola, grants from Biokit, personal fees from Sanofi-Aventis, grants from Fa. Blau Farmaceutics, grants from Prosensa/Biomarin, grants and other from DRK-BSD NSTOB, grants from DRK-BSD Baden-Würtemberg/Hessen, personal fees and non-financial support from Roche, personal fees from GTH e.V.. In addition, Dr. Greinacher reports having a patent, Application no. 2021032220550000DE, pending.

References

1. Voysey, M. *et al.* Safety and efficacy of the ChAdOx1 nCoV-19 vaccine (AZD1222) against SARS-CoV-2: an interim analysis of four randomised controlled trials in Brazil, South Africa, and the UK. *Lancet* **397**, 99–111 (2021).

2. Sadoff, J. *et al.* Safety and Efficacy of Single-Dose Ad26.COV2.S Vaccine against Covid-19. *New Engl J Med* (2021) doi:10.1056/nejmoa2101544.

3. Greinacher, A. *et al.* Thrombotic Thrombocytopenia after ChAdOx1 nCov-19 Vaccination. *New Engl J Med* (2021) doi:10.1056/nejmoa2104840.

4. Scully, M. *et al.* Pathologic Antibodies to Platelet Factor 4 after ChAdOx1 nCoV-19 Vaccination. *New Engl J Med* (2021) doi:10.1056/nejmoa2105385.

5. Huynh, A., Kelton, J. G., Arnold, D. M., Daka, M. & Nazy, I. Antibody epitopes in vaccine-induced immune thrombotic thrombocytopenia. *Nature* 1–7 (2021) doi:10.1038/s41586-021-03744-4.

6. Greinacher, A. *et al.* Towards Understanding ChAdOx1 nCov-19 Vaccine-induced Immune Thrombotic Thrombocytopenia (VITT). (2021) doi:10.21203/rs.3.rs-440461/v1.

7. Krutzke, L., Roesler, R., Wiese, S. & Kochanek, S. Process-related impurities in the ChAdOx1 nCov-19 vaccine. (2021) doi:10.21203/rs.3.rs-477964/v1.

8. Berkers, C. R. *et al.* Activity probe for in vivo profiling of the specificity of proteasome inhibitor bortezomib. *Nat Methods* **2**, 357–362 (2005).

9. EMA. *COVID-19 Vaccine AstraZeneca*. https://www.ema.europa.eu/en/documents/assessment-report/vaxzevria-previously-covid-19-vaccine-astrazeneca-epar-public-assessment-report_en.pdf (2021).

10. Baker, A. T. *et al.* The Structure of ChAdOx1/AZD-1222 Reveals Interactions with CAR and PF4 with Implications for Vaccine-induced Immune Thrombotic Thrombocytopenia. *Biorxiv* 2021.05.19.444882 (2021) doi:10.1101/2021.05.19.444882.

11. Nicolai, L. *et al.* Thrombocytopenia and splenic platelet directed immune responses after intravenous ChAdOx1 nCov-19 administration. *Biorxiv* 2021.06.29.450356 (2021) doi:10.1101/2021.06.29.450356.

12. Hauler, F., Mallery, D. L., McEwan, W. A., Bidgood, S. R. & James, L. C. AAA ATPase p97/VCP is essential for TRIM21-mediated virus neutralization. *Proc National Acad Sci* **109**, 19733–19738 (2012).

13. Bastian, M., Holsteg, M., Hanke-Robinson, H., Duchow, K. & Cussler, K. Bovine Neonatal Pancytopenia: Is this alloimmune syndrome caused by vaccine-induced alloreactive antibodies? *Vaccine* **29**, 5267–5275 (2011).

14. Nickerson, J. L. & Doucette, A. A. Rapid and Quantitative Protein Precipitation for Proteome Analysis by Mass Spectrometry. *J Proteome Res* **19**, 2035–2042 (2020).

15. Blankenburg, S. *et al.* Improving Proteome Coverage for Small Sample Amounts: An Advanced Method for Proteomics Approaches with Low Bacterial Cell Numbers. *Proteomics* **19**, 1900192 (2019).

16. Shevchenko, A., Wilm, M., Vorm, O. & Mann, M. Mass Spectrometric Sequencing of Proteins from Silver-Stained Polyacrylamide Gels. *Anal Chem* **68**, 850–858 (1996).

17. Perez-Riverol, Y. *et al.* The PRIDE database and related tools and resources in 2019: improving support for quantification data. *Nucleic Acids Res* **47**, gky1106- (2018).

18. Schwanhäusser, B. *et al.* Global quantification of mammalian gene expression control. *Nature* **473**, 337–342 (2011).

19. Team, R. D. C. *R: A Language and Environment for Statistical Computing*. (2014).

20. Wickham, H. *et al.* Welcome to the Tidyverse. *J Open Source Softw* **4**, 1686 (2019).

21. Seidel, H. W. and D. *scales: Scale Functions for Visualization.* (n.d.).

22. Provost, A. *et al.* Innovative particle standards and long-lived imaging for 2D and 3D dSTORM. *Sci Rep-uk* **9**, 17967 (2019).

23. Schindelin, J. *et al.* Fiji: an open-source platform for biological-image analysis. *Nat Methods* **9**, 676–682 (2012).

24. Laine, R. F. *et al.* NanoJ: a high-performance open-source super-resolution microscopy toolbox. *J Phys D Appl Phys* **52**, 163001 (2019).

25. Ovesný, M., Křížek, P., Borkovec, J., Švindrych, Z. & Hagen, G. M. ThunderSTORM: a comprehensive ImageJ plug-in for PALM and STORM data analysis and super-resolution imaging. *Bioinformatics* **30**, 2389–2390 (2014).

26. Müller, T. *et al.* Non-muscle myosin IIA is required for the development of the zebrafish glomerulus. *Kidney Int* **80**, 1055–1063 (2011).

27. Xie, J., Farage, E., Sugimoto, M. & Anand-Apte, B. A novel transgenic zebrafish model for blood-brain and blood-retinal barrier development. *Bmc Dev Biol* **10**, 76 (2010).

28. Siegerist, F., Zhou, W., Endlich, K. & Endlich, N. 4D in vivo imaging of glomerular barrier function in a zebrafish podocyte injury model. *Acta Physiol* **220**, 167–173 (2017).

Figures

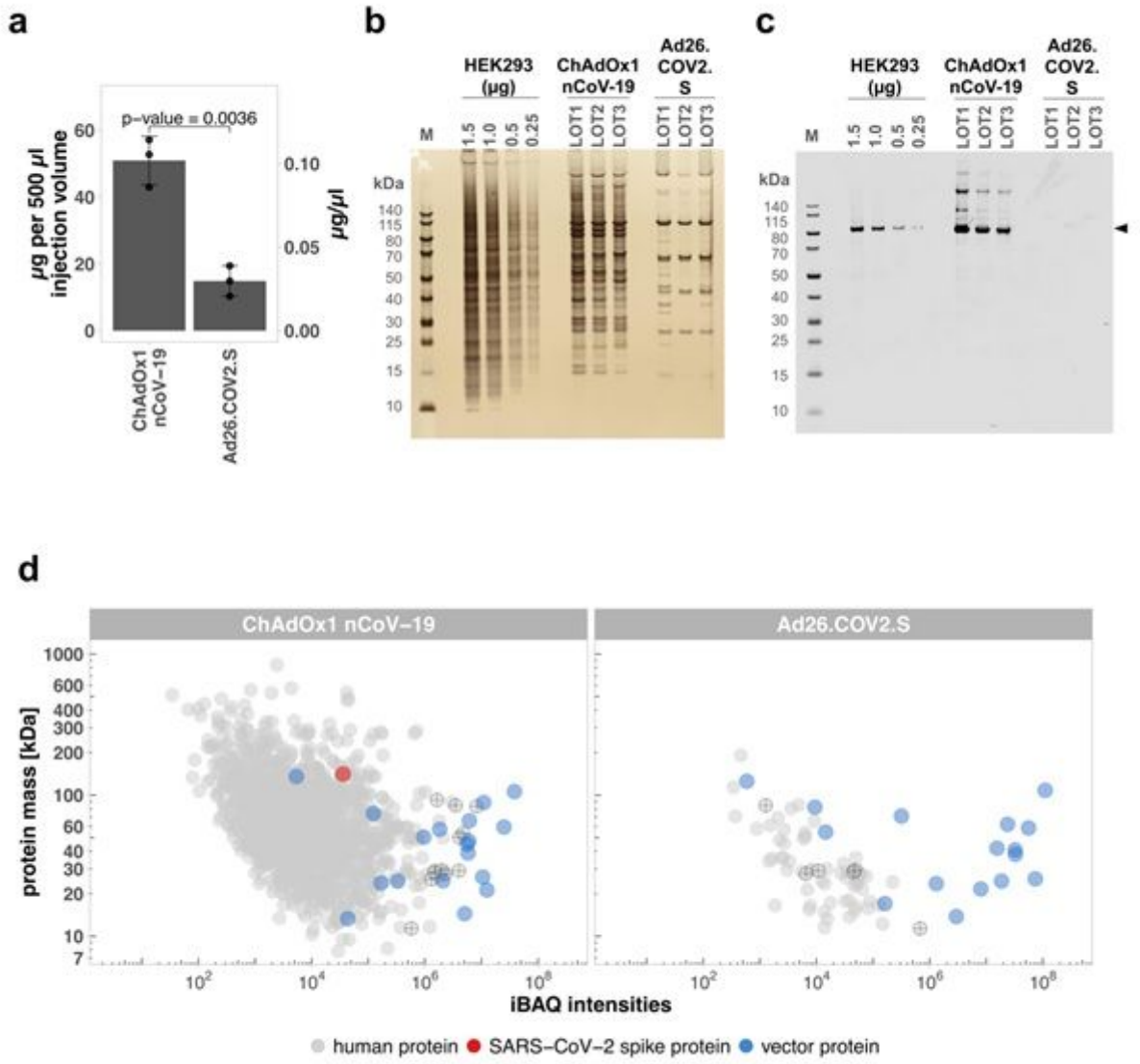

Figure 1

Analysis of the protein composition of ChAdOx1 nCoV-19 and Ad26.COV2.S vaccines (a) Determination of the protein concentration of the two vaccines (3 different LOTs each). Protein concentration was determined with a quantitative BCA assay. Protein concentration per 500 µl (vaccination dose) and 1 µl vaccine (secondary axis) of 3 LOTs of ChAdOx1 nCoV-19 or Ad26.COV2.S vaccine, respectively, are shown. Statistical testing was performed using a two-sided t-test. (b) Protein patterns of silver nitrate-stained SDS-PAGE of ChAdOx1 nCoV-19 or Ad26.COV2.S (3 LOTs each) vaccines along with a dilution series of a laboratory HEK293 cell line extract for comparison. HEK293 cell extract was loaded onto the gel at 1.5, 1.0, 0.5, or 0.25 µg per lane, and 10 µL (1/50th of a vaccine dose) were used for each vaccine. (c) Western blot analysis of HSP90-alpha protein, using the same gel loading scheme as for the silver nitrate-stained gel (A). (d) iBAQ protein intensities and theoretical molecular mass of identified proteins. Protein intensities of ChAdOx1 nCoV-19 or Ad26.COV2.S (exemplarily shown for LOT 3) were calculated using the iBAQ algorithm (minimum of three unique peptides per protein) and plotted against the

theoretical molecular mass. Proteins are color-coded according to their respective class. Blue dots indicate vector proteins; gray dots represent human proteins; the red dot indicates the SARS-CoV-2 spike protein. Points highlighted with a cross indicate proteins additionally analyzed by Western blotting in Suppl. File 1.

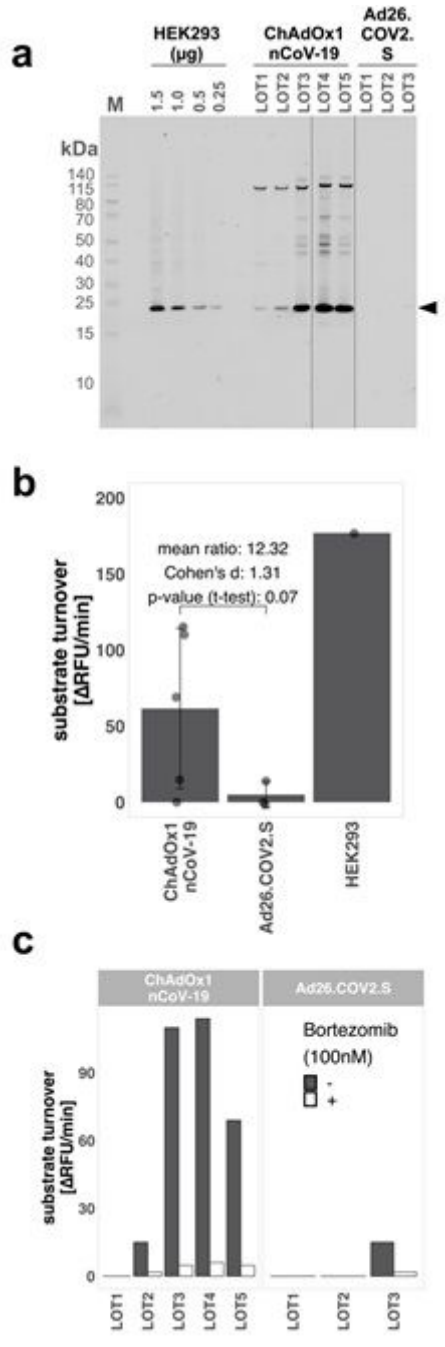

Figure 2

Analysis of proteasome proteins and activity in the vaccines: (a) Western blot analysis of proteasome 20S subunit beta 5 (original Western blot image is provided in Suppl. Fig. 4 a). (b) 50 µl (1/10th of vaccination dose) of different ChAdOx1 nCoV-19 (n=5) and Ad26.COV2.S (n=3) LOTs were analyzed for the chymotrypsin-like activity of the β5-subunit of the proteasome and compared with the activity of 0.25 µg of HEK293 cell lysate (Mean±SD of two technical replicates are shown). (c) Proteasomal activity was

confirmed by inhibition with 100 nM of the β5-subunit-specific inhibitor Bortezomib. The mean of two technical replicates is shown.

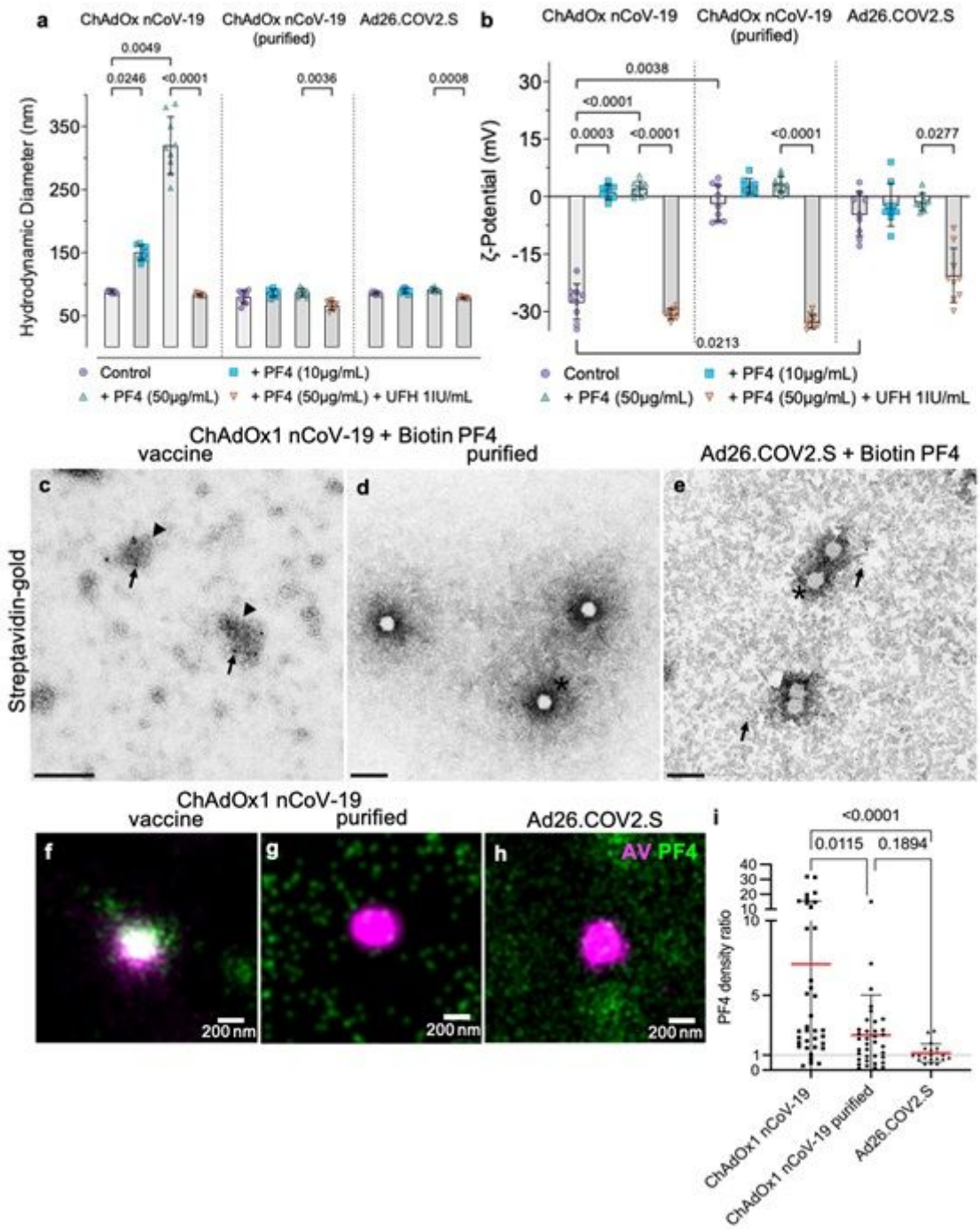

Figure 3

Vaccine-induced PF4 clustering: Analysis of ChAdOx1 nCoV-19, purified ChAdOx1 nCoV-19 virions and Ad26.COV2.S by dynamic light scattering (DLS) (a). The hydrodynamic diameter (mean ± SD, n=9) of ChAdOx1 nCoV-19 or Ad26.COV2.S particles before and after addition of 10 µg/ml or 50 µg/ml PF4 was determined. A dose-dependent increase in the size of ChAdOx1 nCoV-19 aggregates in the presence of PF4 was detected. Addition of unfractionated heparin (1 IU/ml) dissociated previously formed complexes. This effect was markedly reduced in both purified ChAdOx1 nCoV-19 virions and

Ad26.COV2.S. (b) The ζ-potential (mean ± SD, n=9) of ChAdOx1 nCoV-19 was lower than of purified ChAdOx1 nCoV-19 virions or of Ad26.COV2.S; and neutralized by PF4. Panel c-e show representative micrographs of streptavidin-gold immunoelectron microscopy (arrow); biotinylated, human PF4 was incubated with either ChAdOx1 nCoV-19 (c), purified virions from ChAdOx1 nCoV-19 (d) or Ad26.COV2.S (e). Virions are exemplary labeled by asterisks, aggregates by arrowheads; scale bars represent 200 nm. SMLM images in f-h show representative dual PF4 and hexon polypeptide reconstructions after incubation with either ChAdOx1 nCoV-19 (f), purified virions from ChAdOx1 nCoV-19 (g) or Ad26.COV2.S (h). As indicated by the green signal in close proximity to adenoviral particles in (f), PF4 was found in dense clusters after incubation with ChAdOx1 nCoV-19 whereas PF4 formed a more homogeneous layer on glass after incubation with purified ChAdOx1 nCoV-19 (g) or Ad26.COV2.S (h). For quantification, single-molecule particle analysis was performed and particle density ratios (on viral particles / on glass) analyzed (Suppl. Fig. 10). Relative PF4 particle densities are plotted in (i) and showed a statistically significant affinity of PF4 to adenoviral particles predominantly on ChAdOx1 nCoV-19 but not on purified ChAdOx1 nCoV-19 virions or Ad26.COV2.S. Statistical analysis of n=92 particles was performed with Kruskal Wallis test with Dunn's correction for multiple comparisons. Respective p-values are indicated in the plot, red lines and whiskers indicate mean±SD. Dashed line at y=1 (equal affinity of PF4 to adenoviral hexon and glass). Full-field of view images and single-channel reconstructions are provided in Suppl. Fig. 9.

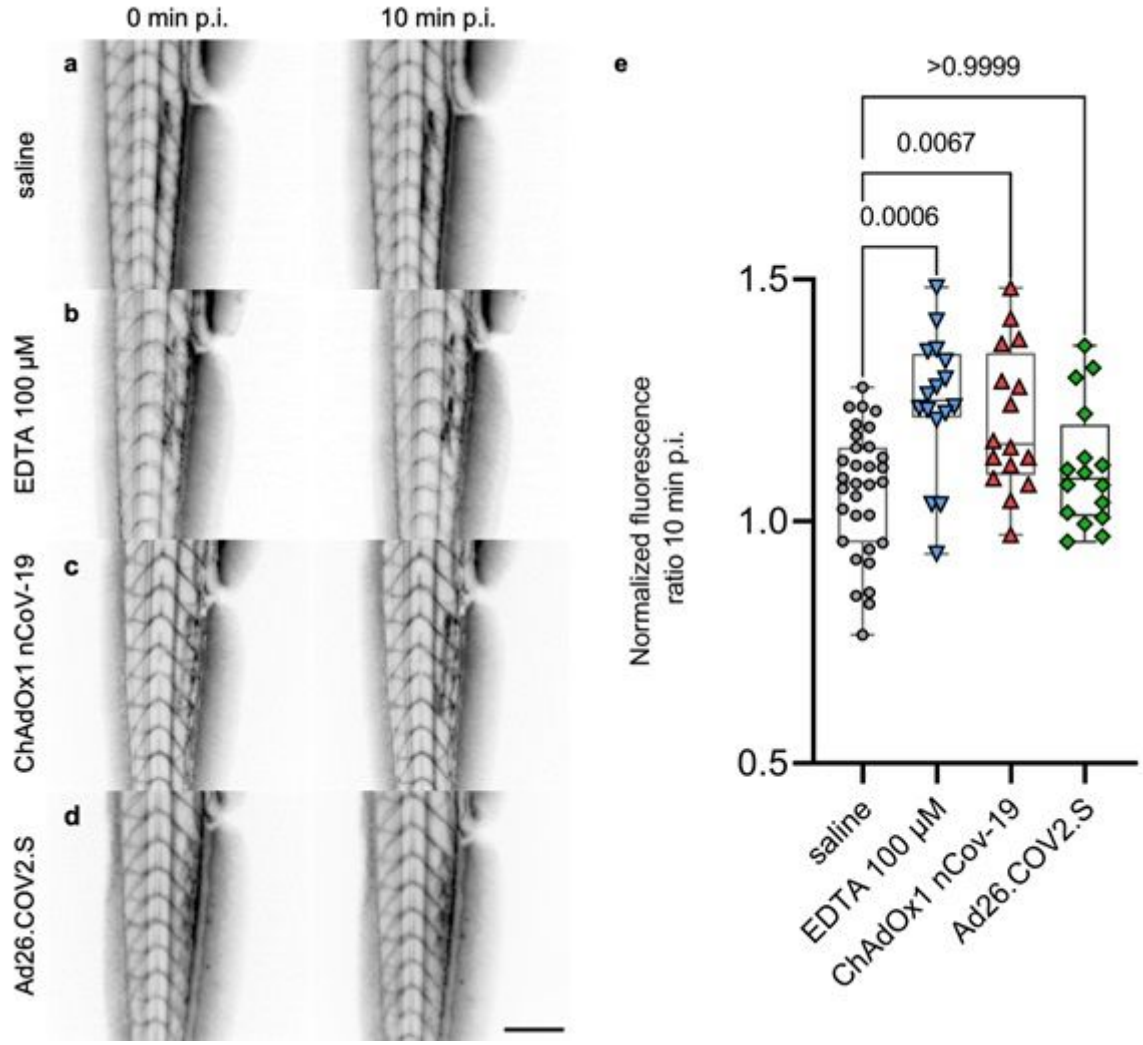

Figure 4

Vascular hyperpermeability assay. Five days past fertilization Tg(-3.5fabp10a:gc-eGFP) zebrafish larvae were microinjected with either physiological saline, 100 µM EDTA, ChAdOx1 nCoV-19, or Ad26.COV2.S in four adjacent myotomes. Local fluorescence intensities of the myotomes were measured at 0 min and 10 min p.i. and normalized to the respective intravascular fluorescence. Injection of 100 µM EDTA, as well as ChAdOx1 nCoV-19, resulted in a significantly elevated extravascular leakage of the 78 kDa gc-eGFP compared to the saline control (a, b, c, e). However, injection of Ad26.COV2.S or physiological saline did not cause an increase of local vascular permeability (a, d, e). Scale bar represents 200 µm.

Supplementary Files

This is a list of supplementary files associated with this preprint. Click to download.

- supplementaltable1iBAQintensitiesfinalTABLE.xlsx
- supplementaltable2iBAQrankedplotofhumanproteinscomparisonTOP10eachTABLE.xlsx
- Supplementalmovie1Intramuscularmicroinjectionsofzebrafishlarvae.mp4
- supplementalfile1Westernblotanalysiscompiled.pptx
- XAZvsJnJsupplementalInformation.docx